

■ **Table S1** Mating design and number of genotypes involved in the analysis per combination in Saint-Appolinaire.

		European larch								Japanese larch									
		104	106	109	166	214	221	222	242	284	3179	3180	3183	3190	3193	3194	3200	3203	3217
European larch	104		12	17	11	9	17	10	5	9	15	13	16	14	14	15	6	12	10
	106	7		12	17		10	20	1	5	16	19	9	10	15	15	13	13	9
	109		5		13	2	12	8	3	4	9	6	2	7	5	15	15	4	6
	166										9	7	1				10		
	214										6	12	5		4	4	9		10
	221	3		6	7	8		12		16	9	4	5	5	16	17	7	5	1
	222				1						9	10		15	19	9	15	11	
	242		19	7	3		8	12			12	14	8	5	12	4	14		13
	284	9	4		3						5	19	3	5	11	10	10	17	4
Japanese larch	3179	4	3	9	11	13	10	11	7			7	7	10	14	10	9	10	8
	3180	6		14	11	8	9		6		7		4	8	10	10	8	6	7
	3183	4	10	15	11	7	10	9	4	14	6	1		10	9	8	7	8	
	3190	1	9	8	14	11	9	5	9	9	2	4	2		7	1		8	7
	3193	6	5	5	15	5	4		7		4	4	6	5		2	14	14	12
	3194				7				6		8	7			9			12	7
	3200						6					8	8	2	5	1			
	3203	8	6	16	7	13	14		9	1	8	14	1	3	3	7	2		6
	3217	10	10	14	15		19		7		12	13	13	2	8	12	13	12	

■ **Table S2** Mating design and number of genotypes involved in the analysis per combination in Saint-Saud.

		European larch								Japanese larch									
		104	106	109	166	214	221	222	242	284	3179	3180	3183	3190	3193	3194	3200	3203	3217
European larch	104		24	22		11	26			18	26	26	22	22	28	26	18	20	28
	106	22		23	24		8	26		7	21	26	20	16	26	23	12	24	
	109				11		12	8						11		18	17		4
	166										5	10					15		
	214																11		8
	221			3						19				7	26	10	9		
	222										27	12		27	18	11	23	12	
	242		27					8	12		21	11		10	22		25		22
	284											13			11	10	8	14	
Japanese larch	3179			26	11	27		28				18	18	22	25	23	12	22	20
	3180										22			4	13	21	10		
	3183		24	19	21		9	9			26	8		16	15	20	15	14	
	3190		10		18	10	10	10			9				8			21	7
	3193		8		12								17	5			17	25	12
	3194										8				14			29	10
	3200																		6
	3203	9	15	26		11	22		11			25					9		
	3217	28		14	13		28				19	29	11	8	6	28	21	18	

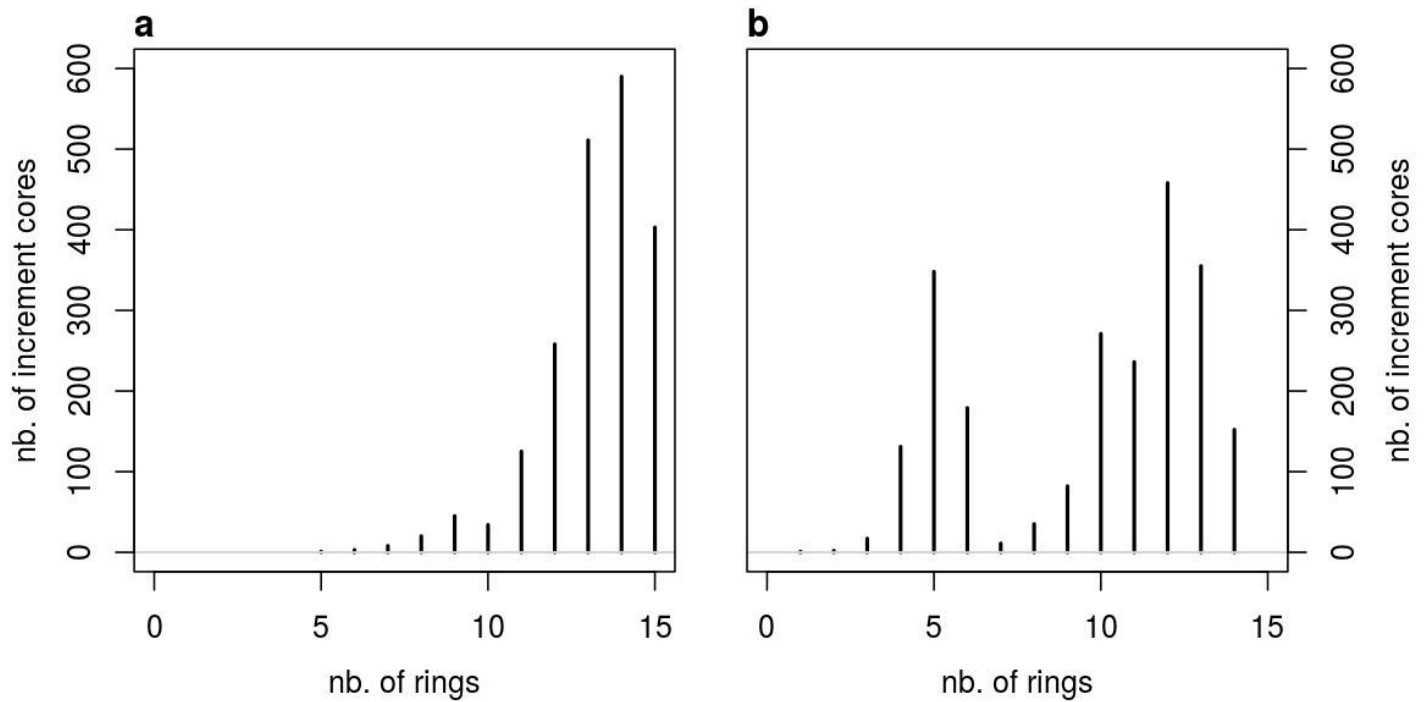


Figure S1 Number of rings per increment cores from Saint-Appolinaire (a) and from Saint-Saud (b)

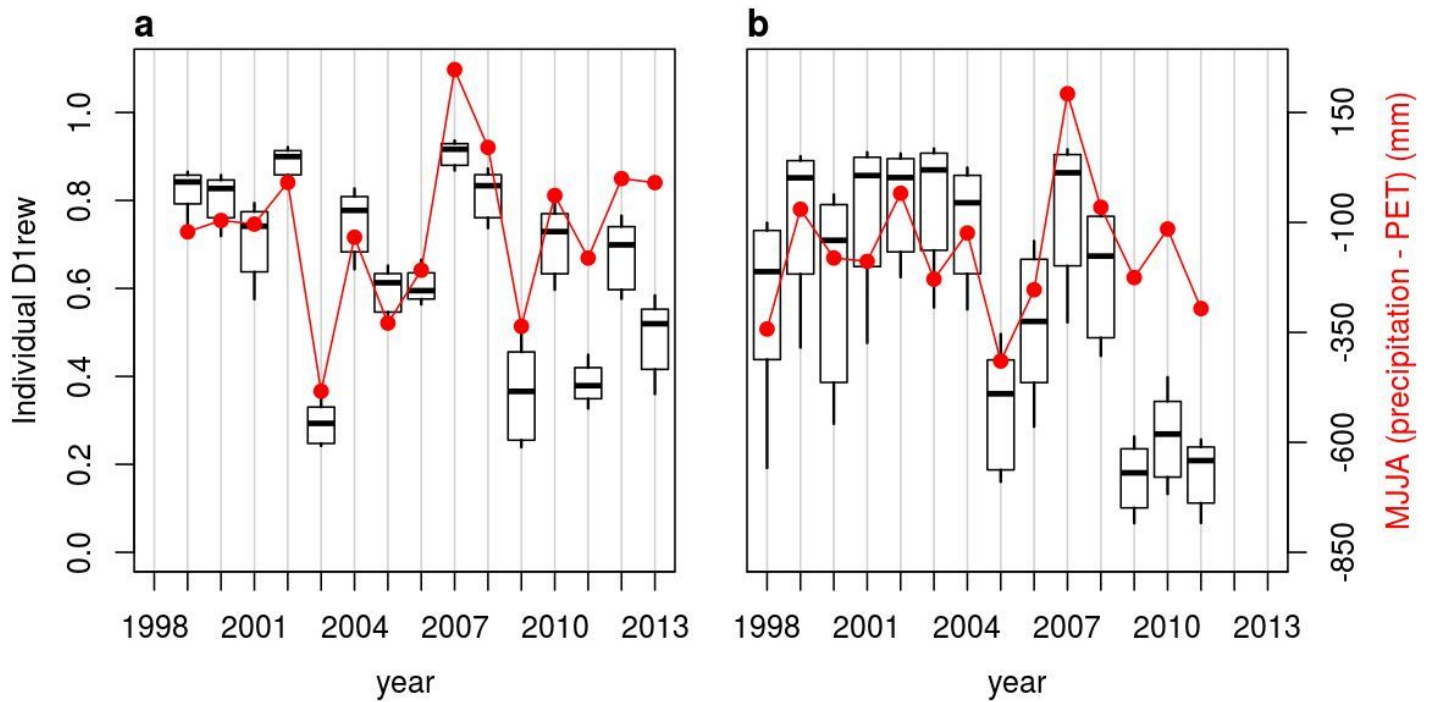


Figure S2 In black: boxplots of the distribution of individual D1rew (first decile of the daily relative extractable water) for each year in each site SA (a) and SS (b). In red: the simpler index MJJA, defined as the sum of the daily differences between precipitation and potential evapotranspiration from May to July

970 **Leaf area index**

971 The leaf area index (LAI) is the ratio of leaves surface per ground surface. Thus in a growing stand the LAI is expected to increase, and
 972 this plays an important role in the water balance model, as detailed further. The LAI can be calculated from the basal area, that is, the
 973 surface of cross-section of tree stems per ground surface. Basal area was calculated in each site at each age for which we had a breast-height
 974 circumference (BHC) measurement. We estimated transmittance from basal area and age using [Sonohat *et al.* \(2004\)](#) ('Model 2', $R^2 = 0.867$):

$$\tau = \exp\left(-b_{max}\left(\frac{age}{age_{max}}\exp\left(1 - \frac{age}{age_{max}}\right)\right)^p G\right)$$

975 where G was the basal area, and age_{max} , p , and b_{max} the model parameters available in [Sonohat *et al.* \(2004\)](#). From transmittance we could
 976 estimate the LAI as $LAI_{max} = -\ln(\tau)/k$ with the value $k = 0.6$ for larch ([Takeda *et al.* 2008](#)). The index 'max' in LAI_{max} means: the LAI
 977 when the vegetation is maximal in the season. Then, we linearly inferred the LAI_{max} at any age for which we had ring observations. The
 978 LAI_{max} was inferred at the site scale. We present the calculated and the inferred LAI_{max} in [Fig. S3](#).

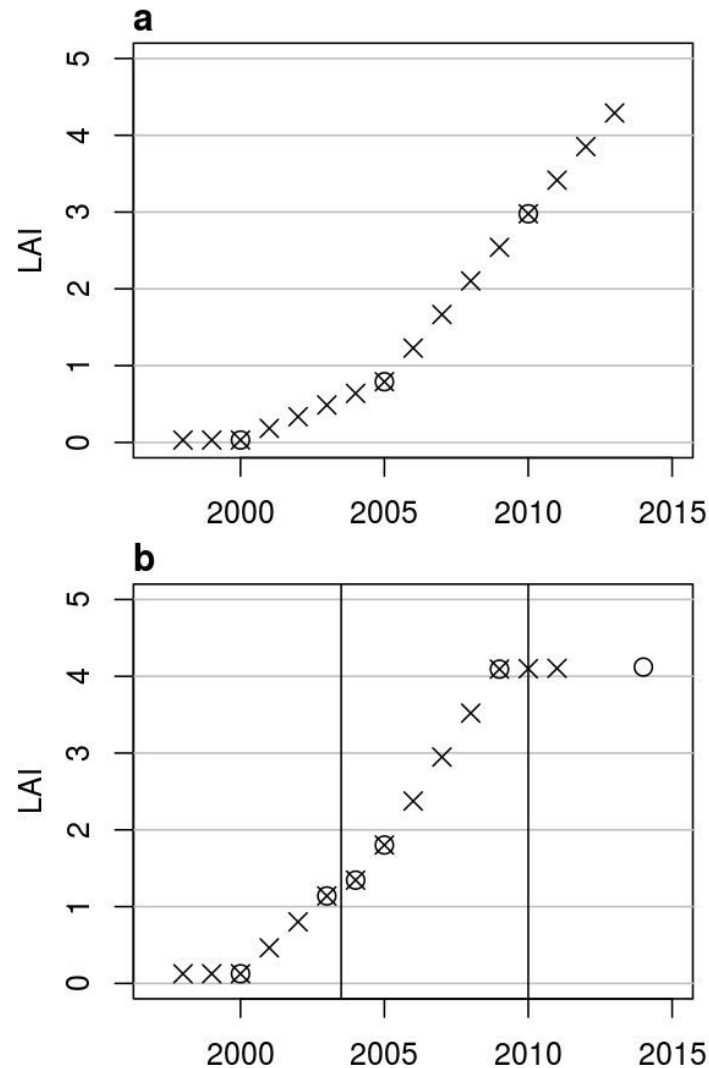


Figure S3 LAI_{max} evolution in each site: SA (a) and SS (b). Circles: LAI_{max} estimated from basal area. Non-circled crosses: LAI_{max} linearly inferred. All crosses: LAI_{max} used in the water balance model

979 **Soil available water capacity**

980 We excavated 2 pits in SA and 3 pits in SS, in the most contrasted areas. The contrasted areas were assessed using tree height (at the last
 981 age available) spatial effect maps. The spatial effects were predicted as best linear unbiased predictions (BLUPs) from model 'M1' in
 982 [Marchal *et al.* \(2017\)](#). In each pit, we measured soil horizon thickness, stone content, and we collected samples to assess the soil texture. We
 983 estimated the available water capacity (AWC) for each pit ([Bruand *et al.* 2004](#)), that is, the maximal amount of water available for plants
 984 that the soil can store. We assumed that height spatial effect informed on AWC, as empirically supported in [Fig. S4](#). Within each site, we

985 considered a linear relation between tree height spatial effects (BLUPs) and AWC in order to infer AWC at the tree level. Nevertheless, for
 986 each site, we prevented the individual trees AWC from being lower (or higher) than the lowest (or highest) pits' AWCs, resulting in an
 987 inverse-M shaped distribution.

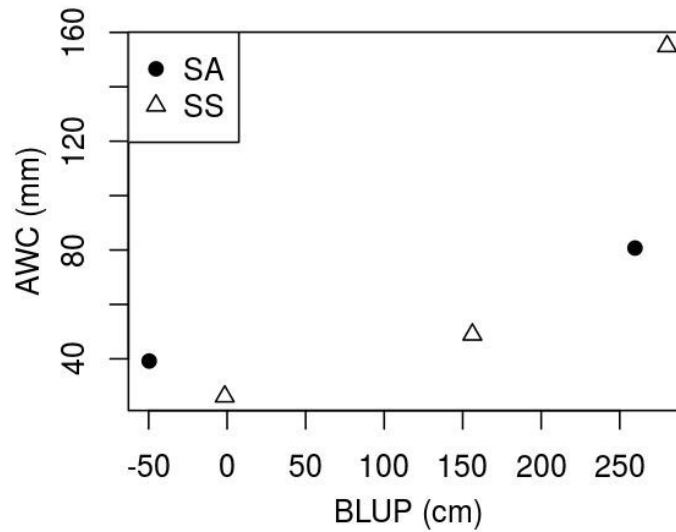


Figure S4 Link between height spatial effect (estimated as a best linear unbiased predictor, BLUP) and the available water capacity (AWC) in each site: Saint-Appolinaire (SA, black dots) and Saint-Saud (SS, white triangles). Each dot represents a pit

988 Climatic data

989 The daily climate information we used were the precipitations (P) and the potential evapotranspiration (PET). Raw climatic data were from
 990 Météo-France, via the platform INRA CLIMATIK which computed the PET with Penman-Montheith method. Ten PET data points were
 991 missing in SS, we imputed them using an autoregressive model (Muñoz and Sánchez 2015) with an autocorrelation parameter $\rho = 0.95$.

992 Water balance model and water availability indexes

993 We used an adapted, simplified implementation of Granier *et al.* (1999)'s daily water balance model. We simplified the model as follows: (i)
 994 we proposed a simplified formulation for the understorey evapotranspiration; (ii) we proposed a simplified formulation for the rainfall
 995 interception; (iii) we ignored soil stratification and distribution of the roots, so only the overall AWC described the subsoil. The daily water
 996 balance was:

$$997 \quad (\text{Granier et al. 1999, eq. 1}) \Delta W = P - In - T - Eu - D$$

998 with W : the soil water content and ΔW its daily variation; P : the precipitation; In : the rainfall interception; T : the overstorey transpiration;
 999 Eu : the understorey evapotranspiration; and D : the drainage; all expressed in mm. The relative extractable water (REW) content in soil
 1000 was calculated as $REW = W / AWC$. The LAI was 0 until day 105 (15th of April for a non-leap year), then increased linearly in 30 days,
 1001 stayed at LAI_{max} a while and finally decreased linearly to 0 in 30 days, finishing the decrease at day 288 (15th of October). The canopy
 1002 transpiration T was calculated as following:

$$1003 \quad (\text{Granier et al. 1999, eq. 2}) T_{max} = r_T * PET \text{ with } \begin{cases} r_T = 0.125 * LAI \text{ if } LAI < 6 \\ r_T = 0.75 \text{ otherwise} \end{cases}$$

1004 If REW was above 0.4 (considered as a drought threshold), T was T_{max} . Otherwise, T decreased linearly with REW. We used no intercept
 1005 to the linear relation between T and REW, so that the transpiration was null if no water was available. The drainage D was such as REW
 1006 was never above 1. We proposed the following method for Eu :

$$Eu_{max} = r_{Eu} * PET * \exp(-k * LAI)$$

1007 with $k = 0.6$ for larch (Takeda *et al.* 2008); then Eu was calculated from Eu_{max} the same way T was calculated from T_{max} . Using a model
 1008 derived from Penman-Montheith equations, Kelliher *et al.* (1995) represented the relation between G_s/G_c and the LAI; with G_s the
 1009 understorey surface conductance and G_c the tree canopy conductance. This relation is plotted in Fig. S5. We also present in Fig. S5 the
 1010 ratio $(Eu + T) / T$ depending on r_{Eu} . It arises from this comparison that $r_{Eu} = 0.375$ provides water flow ratios that are consistent with the
 1011 conductance ratios from Kelliher *et al.* (1995), especially in the condition of low LAI. Therefore, we used $r_{Eu} = 0.375$ to parameterize the
 1012 model during the growth season. In order to account for the decrease in the overstorey biological activity in winter, r_{Eu} was set to 0.125
 1013 between the days 288 and 105 with 30 days of linear transition (just as the trees LAI varying from LAI_{max} to 0).

1014 In order to model the water losses by rainfall interception we introduced a new compartment, the tree canopy water storage S .
 1015 This compartment was limited by S_{max} , the total amount of water that the canopy could store, which was set as a function of the LAI:

1016 $S_{max} = 3 \text{ mm} * (1 - \exp(-k * LAI_{max}))$. The value 3 mm and the absence of seasonal variation for the canopy water storage capacity were
1017 specific to larch (Reynolds and Henderson 1967). The interception algorithm was unsophisticated: S was filled first, then when it was full
1018 the extra water dropped to the ground. We applied the following rules adapted from Granier *et al.* (1999): (i) The canopy transpiration T
1019 was reduced by 20% of S and (ii) the sum of T , Eu and the evaporation from S was limited to 1.2 times the PET . Finally, the remaining
1020 water on the leaves was transferred to the next day.

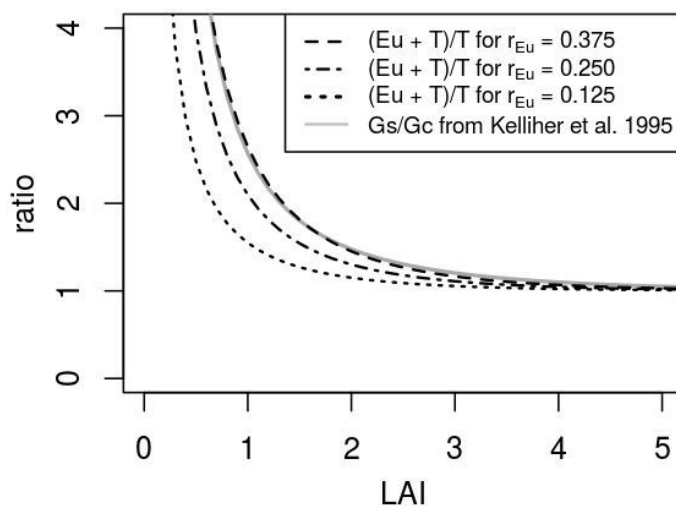


Figure S5 Ratio between the water transpired by tree canopy (T) and evapotranspired by the understory vegetation (Eu), and ratio between understory vegetation conductance (Gs) and tree canopy conductance (Gc) as modeled by Kelliher *et al.* (1995), depending on the leaf area index (LAI)

1022 A locus-based simulation software (Metagene) using a finite loci approach was previously developed at INRA (Sánchez *et al.* 2008,
 1023 <http://www.igv.fi.cnr.it/noveltree>). The initial software was adapted to the study of forest tree breeding strategies dealing with adverse
 1024 genetic correlations (Hallingbäck *et al.* 2014), or long-term genetic diversity issues (Wu *et al.* 2016). It was further expanded for the present
 1025 study to simulate heritable traits responding longitudinally to environmental variations. According to the phenotypic plasticity literature
 1026 (Windig *et al.* 2004; Pigliucci 2005), two nonexclusive genetic mechanisms can be assumed for modeling a plastic response: 'epistatic'
 1027 plasticity and 'pleiotropic' plasticity. Briefly, while epistatic plasticity denotes mainly the causal mechanism by which regulatory genes
 1028 serve as environmentally operated signal boxes for switching between alternative genetic pathways, the pleiotropic plasticity concept
 1029 refers to genes that have pleiotropic effects on a given character expressed in different environments. Both mechanisms were coded as
 1030 available gene actions in the simulator, but only the latter was used in this study for simplicity. Thus, the effect of a locus was set as a
 1031 function of a given environmental gradient x . Rather than prospecting the effects of underlying genetic architectures and mechanisms on
 1032 the plastic response, our main objective here was to produce with a reasonably simple setup heritable reaction norms.

1033 Therefore, our modeling of plastic responses relied on loci with alleles showing environmental sensibility in their genetic effects. For this,
 1034 genotypic values were modeled by a quadratic function such as $\alpha(x) = \alpha_0 + \alpha_1(x + \delta) + \alpha_2(x + \delta)^2$, where parameters α_0 , α_1 , α_2 and δ
 1035 defined a genotypic reaction norm with a certain parabolic shape over the range of the environment x . Each locus required two of these
 1036 functions, one for the favorable homozygote (AA) and another for the unfavorable homozygote (aa), with heterozygote (Aa) being always
 1037 intermediate (*i.e.* no dominance). Averaged allele effects were further computed following Falconer and Mackay (1996). Underlying the
 1038 plastic trait, we considered 30 diallelic loci with alternating quadratic functions across the genome between two possible parametric sets
 1039 (first set, AA: $\alpha_0 = 0$, $\alpha_1 = 2$, $\alpha_2 = 0$; aa: $\alpha_0 = 0$, $\alpha_1 = -1$, $\alpha_2 = 0$; and second set, AA: $\alpha_0 = 0$, $\alpha_1 = 0$, $\alpha_2 = 2$; aa: $\alpha_0 = 0$, $\alpha_1 = 0$, $\alpha_2 = -3$).
 1040 The δ parameter was locus specific and varied between -0.7 and 0.75 across the genome, in such a way that a certain level of heterogeneity
 1041 in $\alpha(x)$ when $x \rightarrow 0$ was produced. The environmental deviate, x , was randomly sampled from a normal distribution (mean = 0 and
 1042 standard deviation = 0.2) to obtain a set of n environments, equal to the number of sibs per mating.

1043 All loci were considered to be evenly spaced across the genome, and recombination occurred without interference considering an
 1044 arbitrary genome size of 600 cM. The initial sample of alleles that made up founder genotypes was randomly drawn from a distribution
 1045 where allelic frequencies could be set randomly across loci within a range between 0.2 and 0.8. Individual genotypic values per environment
 1046 were the result of the sum of all loci's genotypic contributions for the corresponding environment. The corresponding phenotypic value,
 1047 expressed in a given environment x , was the sum of the genotypic value and a residual deviation which was sampled from $N(0,$
 1048 $\sigma_R^2(x) = \sigma_A^2(x)(\frac{1}{h^2} - 1))$ where $\sigma_A^2(x)$ was the additive variance at the x environment, and h^2 the initial narrow-sense heritability being
 1049 constant along the environmental gradient. Note that the residual deviation was not correlated to the environmental cue x .

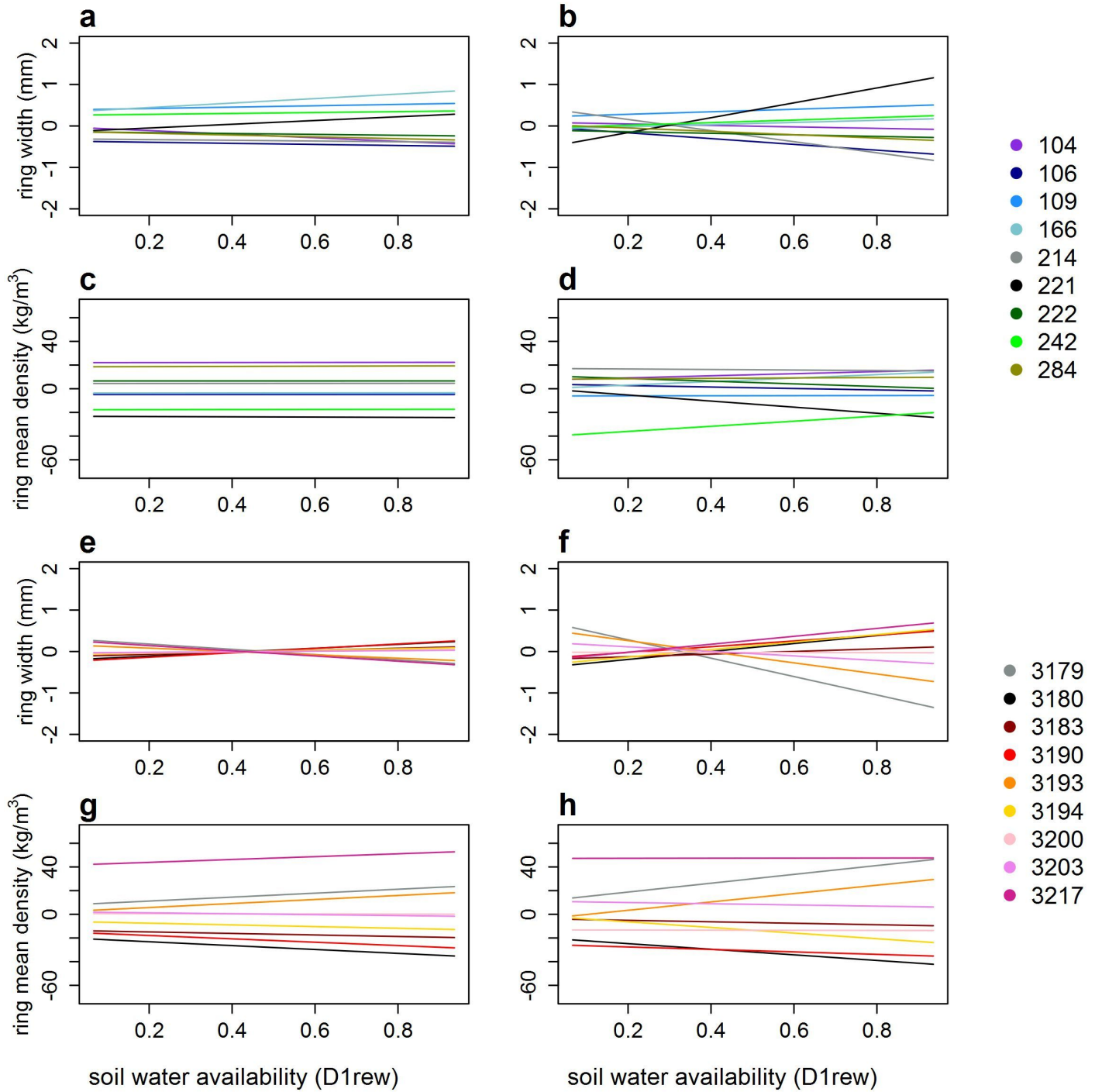


Figure S6 Genetic performances for the 9 European larch parents (a-d) and the 9 Japanese larch parents (e-h) for ring width (a-b, e-f) and ring mean density (c-d, g-h), in pure species (breeding value) (a, c, e, g) and in hybridization (twice the general hybridization ability) (b, d, f, h), along the first decile of the daily relative extractable water (D1rew). Each color represents one genotype, labeled in the legend on the right

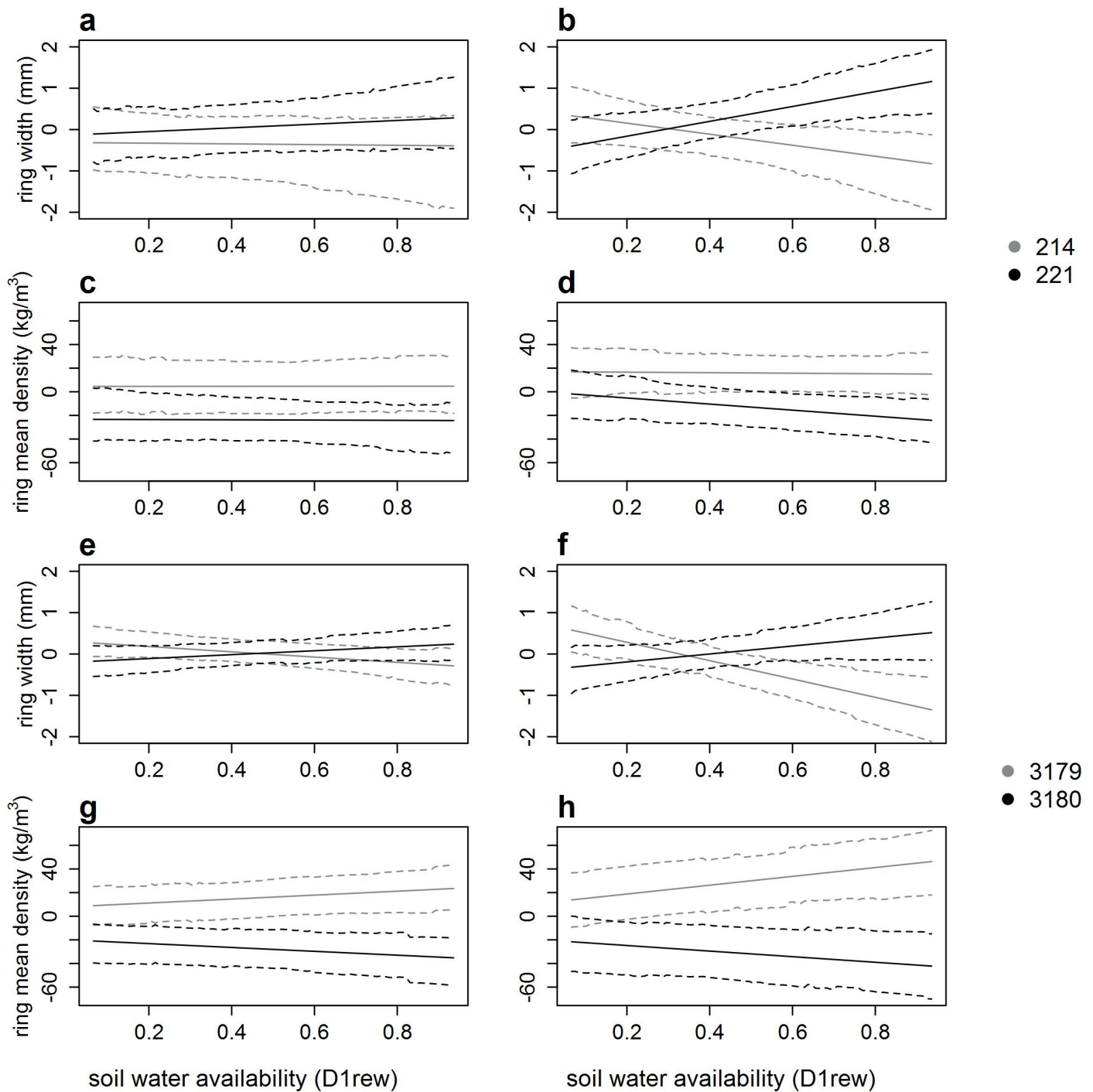


Figure S7 Genetic performances with 95% CIs (dashed lines) for some contrasted European larch parents (a-d) and Japanese larch parents (e-h) for ring width (a-b, e-f) and ring mean density (c-d, g-h), in pure species (breeding value) (a, c, e, g) and in hybridization (twice the general hybridization ability) (b, d, f, h), along the first decile of the daily relative extractable water (D1rew). Each color represents one genotype, labeled in the legend on the right

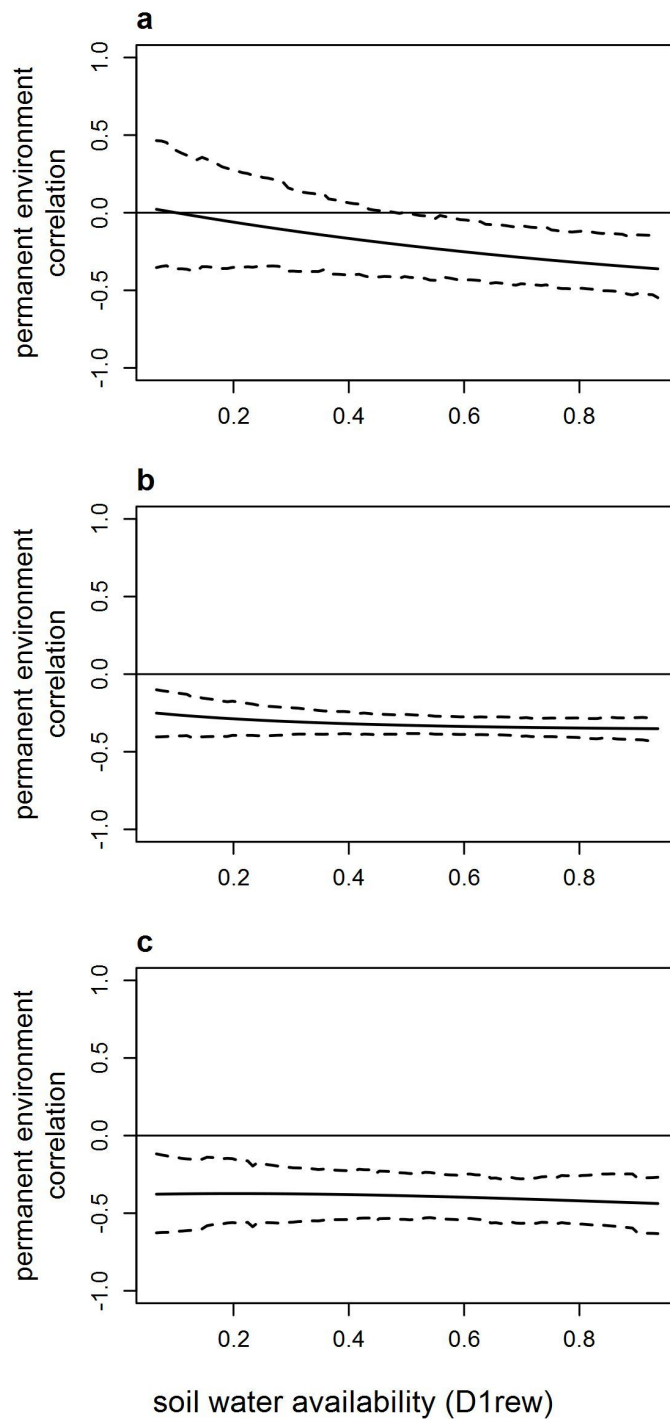


Figure S8 Permanent environment correlations between ring width and ring mean density along the first decile of the daily relative extractable water (D1rew), for European larch (a), hybrid larch (b) and Japanese larch (c). These correlations were computed from the variance and covariance parameters estimated with the multivariate, order 1 random regressions. Dashed lines: 95% CIs

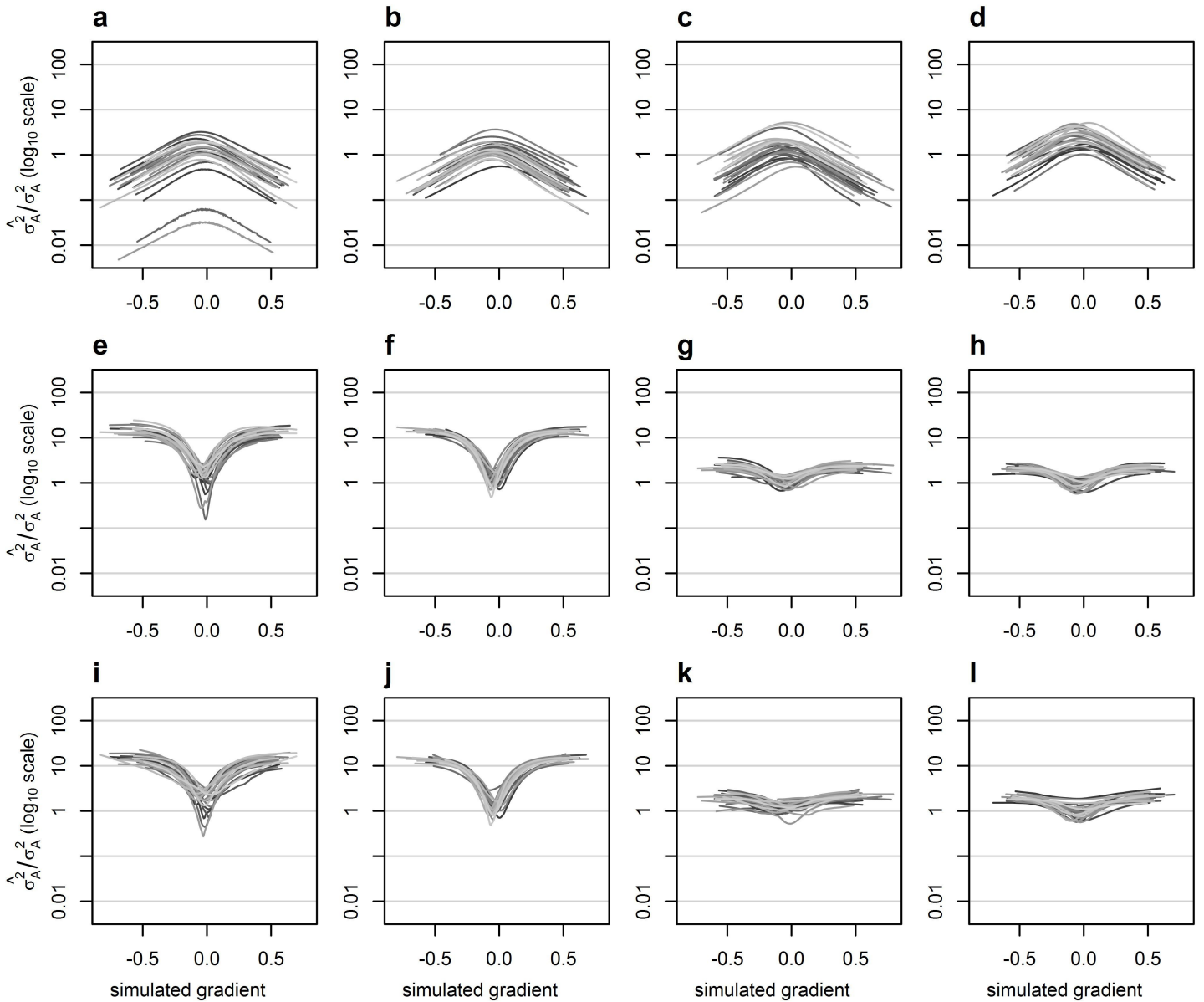


Figure S9 Ratio between the estimated additive variances and the true variances for each simulated scenario: (1) $h^2 = 0.1$ and $n = 20$ (a, e, i), (2) $h^2 = 0.1$ and $n = 120$ (b, f, j), (3) $h^2 = 0.6$ and $n = 20$ (c, g, k), and (4) $h^2 = 0.6$ and $n = 120$ (d, h, l); for 100 simulations in each scenario, and for each order of random regression: order 0 (a-d), order 1 (e-h) and order 2 (i-l). Each grey curve is the ratio for 1 simulation

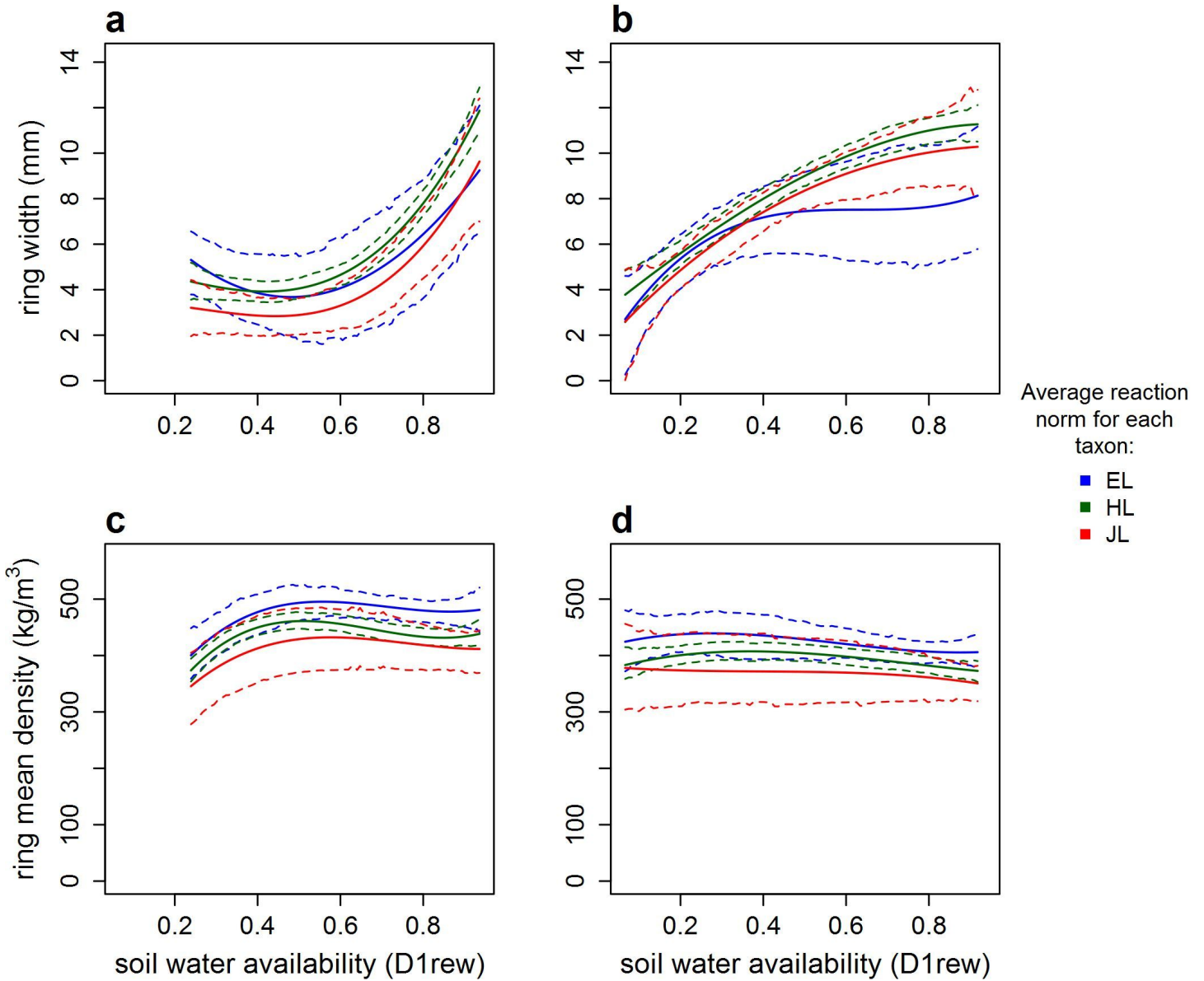


Figure S10 Taxa average reaction norms as in Fig. 4, predicted using a single observation per tree, for traits ring width (a, b) and ring mean density (c, d) along D1rew, in the sites SA (a, c) and SS (b, d), for European larch (in blue, EL), Japanese larch (in red, JL) and the hybrid (in green, HL)). Dashed lines: 95% credible intervals